^{56,54}Fe$(n, \alpha)^{53,51}$Cr cross sections in the MeV region

Huaiyong Bai,[1] Haoyu Jiang,[1] Yi Lu,[1] Zengqi Cui,[1] Jinxiang Chen,[1] Guohui Zhang,[1,*] Yu. M. Gledenov,[2] M. V. Sedysheva,[2] G. Khuukhenkhuu,[3] Xichao Ruan,[4] Hanxiong Huang,[4] Jie Ren,[4] and Qiwen Fan[4]

[1]*State Key Laboratory of Nuclear Physics and Technology, Institute of Heavy Ion Physics, Peking University, Beijing 100871, China*

[2]*Frank Laboratory of Neutron Physics, Joint Institute for Nuclear Research, Dubna 141980, Russia*

[3]*Nuclear Research Centre, National University of Mongolia, Ulaanbaatar, Mongolia*

[4]*China Institute of Atomic Energy, Beijing 102413, China*

(Received 28 April 2018; published 26 February 2019)

^{56,54}Fe$(n, \alpha)^{53,51}$Cr cross sections were measured in the neutron energy region of 5–11 MeV using three neutron sources based on accelerators, a twin gridded ionization chamber, and highly enriched ^{56}Fe and ^{54}Fe foil samples. The ^{238}U(n, f) reaction was used to monitor the neutron fluence, and the interferences from the low-energy neutrons were corrected according to the neutron energy spectra obtained through unfolding the pulse height spectra measured by a liquid scintillator. Both the measured cross sections show a "shoulder" structure in the 8–11 MeV region which may be caused by the level structure of the residual nuclei. The present paper aims to improve constraint of the ^{56,54}Fe$(n, \alpha)^{53,51}$Cr excitation functions in the MeV region where their neutron energy dependences are significant, while related measurements are nonexistent or scarce and the deviations among existing measurements and evaluations are significant. To obtain more precise excitation functions of the ^{56,54}Fe$(n, \alpha)^{53,51}$Cr reactions, further measurements and improved evaluations are required.

DOI: 10.1103/PhysRevC.99.024619

I. INTRODUCTION

Iron is one of the most important structural materials for accelerators and nuclear reactors. The abundances of ^{56}Fe and ^{54}Fe in natural iron are 91.754 and 5.845%, respectively. When irradiated by fast neutrons, helium will be accumulated through the ^{56,54}Fe$(n, \alpha)^{53,51}$Cr reactions, which will cause embrittlement problems [1,2]. Therefore, accurate cross sections of the ^{56,54}Fe$(n, \alpha)^{53,51}$Cr reactions are crucial to evaluate the irradiation damages of nuclear facilities. From the theoretical point of view, the cross sections of the ^{56,54}Fe$(n, \alpha)^{53,51}$Cr reactions can also provide related information on the shell effect, since the numbers of both protons and neutrons in ^{56}Fe and ^{54}Fe are close to the magic number of 28 [3,4].

Existing measurement results for the ^{56}Fe$(n, \alpha)^{53}$Cr reaction are scarce because ^{53}Cr is stable and the commonly used activation method is not available. In the EXFOR library [5], there are only two measurements including one energy point at 8.0 MeV (Saraf *et al.*) and four energy points in the 4.0–6.5 MeV region (Wang *et al.* [1]). The latter was finished by our group [1], and our results are obviously higher than that of Saraf *et al.*'s. As a result, discrepancies among different evaluations are bigger than 100% in the MeV region [6].

For the ^{54}Fe$(n, \alpha)^{51}$Cr reaction, although existing measurements are abundant since the activation method is available, measurements in the 7–13 MeV region are still lacking because it is difficult to obtain monoenergetic neutrons in this region. As a result, discrepancies among different measurements and evaluations in the 7–13 MeV region are apparent. Results of the recent integration measurement [7] using a ^{252}Cf neutron source show that the cross sections of the ^{54}Fe$(n, \alpha)^{51}$Cr reaction in ENDF/B-VII.1, JENDL-4, and CENDL-3.1 libraries are higher by 12.7–17.6% than that of the measurement. Furthermore, in the measurement of Meadows *et al.* [8], the ^{54}Fe$(n, \alpha)^{51}$Cr reaction cross sections show a "shoulder" structure in the 8–11 MeV region which is absent in almost all the evaluations. So, new measurements of the ^{54}Fe$(n, \alpha)^{51}$Cr reaction are required to constrain the excitation function and to validate the shoulder structure.

In the present paper, the ^{56,54}Fe$(n, \alpha)^{53,51}$Cr cross sections were measured at five energy points in the 5–11 MeV region. The experiments are illustrated in Sec. II, the data processing and the results are presented in Sec. III, and conclusions are drawn in Sec. IV.

II. DETAILS OF THE EXPERIMENTS

The sketch of the experimental setup is illustrated in Fig. 1, which is composed of three main parts: the neutron source, the charged particle detector, and the data acquisition system. Compared with our previous work [1], four improvements were adopted in the present measurements. First, the neutron energy spectra were measured using a liquid scintillator detector [9], so that the interference from the low-energy neutrons can be corrected. Second, the Xe + 5.0% H_2 mixtures were used as the working gas of the gridded ionization chamber instead of Kr + 2.7% CO_2 mixtures, so that the strong background from the ^{16}O$(n, \alpha)^{13}$C reaction in the high neutron energy region can be excluded. Third,

*Corresponding author: guohuizhang@pku.edu.cn

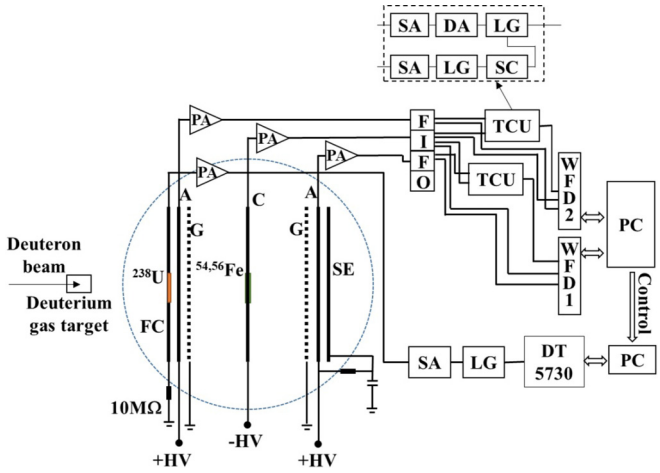

FIG. 1. The sketch of the experimental setup: FC, fission cathode; PA, charge sensitive preamplifier; A, anode; G, grid; C, cathode; SE, shielding electrode; FIFO, fan in–fan out (CAEN N625); TCU, trigger control unit; SA, signal amplifier (ORTEC 572A); DA, delay amplifier (ORTEC 427A); LG, linear gate (ORTEC 542); SC, single channel analyzer (ORTEC 551); WFD, waveform digitizer (Signatec PDA14); DT5730, desktop digitizer (CAEN DT5730B); and PC, personal computer.

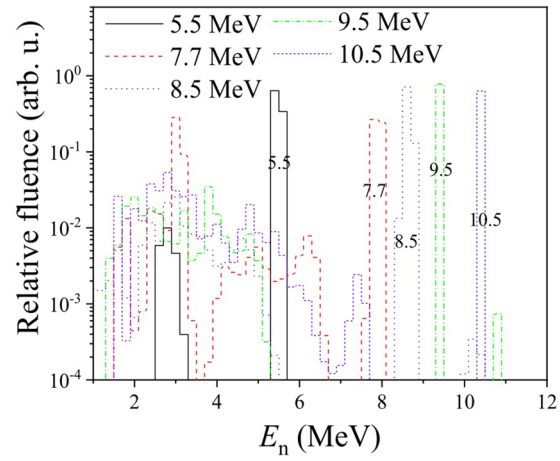

FIG. 2. The measured neutron energy spectra.

the ^{238}U sample [10] was moved from the cathode to the fission cathode of the gridded ionization chamber, and the counts of the fission fragments from the ^{238}U(n, f) reaction were used instead of the BF_3 counts [11] for normalization in the background deduction. The normalization factor provided by the fission counts was more accurate than that provided by the BF_3 counts [12]. Finally, the updated data acquisition system based on waveform digitizers was utilized instead of the nuclear instrument module based data acquisitions [13]. These upgrades made the precise measurement of the ^{56,54}Fe$(n, \alpha)^{53,51}$Cr cross sections in the 7–11 MeV region possible, because the interferences from low-energy neutrons can be deducted, the strong background of the working gas can be greatly decreased, and a more accurate normalization factor in the background deduction can be obtained.

In the present paper, three neutron sources based on accelerators were used as presented in Table I. First, to verify the present measurement method, the ^{56,54}Fe$(n, \alpha)^{53,51}$Cr reaction cross sections were remeasured at 5.5 MeV based on the 4.5-MV Van de Graaff accelerator of Peking University (PKU). The neutrons were produced through the D$(d, n)^3$He reaction using a deuterium gas target 2.0 cm in length and ~0.30 MPa in pressure. The deuterium gas target was separated from the vacuum tube of the accelerator by a molybdenum foil 5 μm in thickness. Second, measurements were extended to 7.7 MeV based on the 4.5-MV Van de Graaff accelerator of PKU. The neutrons were generated through the ^{9}Be$(\alpha, n)^{12}$C reaction using a solid beryllium target ~ 500 μg/cm^2 in thickness. Finally, measurements were performed at 8.5, 9.5, and 10.5 MeV based on the HI-13 tandem accelerator of China Institute of Atomic Energy (CIAE). The neutrons were generated through the D$(d, n)^3$He reaction using a deuterium gas target 3.0 cm in length and ~0.25 MPa in pressure. The deuterium gas target was separated from the vacuum tube of the accelerator by a molybdenum foil 10 μm in thickness. The corresponding neutron energy spectra (shown in Fig. 2) were measured using an EJ309 liquid scintillator detector placed at 0° with respect to the beam line by unfolding the measured pulse height spectra [9]. Although the folded back pulse height spectra of the obtained neutron energy spectra agreed well with the measured ones (relative deviation <3%), the uncertainties of the proportions of the low-energy neutrons were assumed to be 10% to make sure that they were reliable within the uncertainties. With the ^{238}U(n, f) excitation function taken from Ref. [14], the measured neutron energy spectra, and the corresponding angular differential cross sections introduced below, the fission proportion ρ_L induced by low-energy neutrons can be subtracted. The D$(d, n)^3$He and D(d, np)D angular differential cross sections were taken from the ENDF/B-VIII.b3 library [6] and Ref. [15], separately. The ^{9}Be$(\alpha, n_0)^{12}$C and ^{9}Be$(\alpha, n_1)^{12}$C

TABLE I. Descriptions of the neutron sources.

Energy (MeV)	5.5	7.7	8.5, 9.5, and 10.5
Reaction	D$(d, n)^3$He	^{9}Be$(\alpha, n)^{12}$C	D$(d, n)^3$He
Target	Gas target, 2.0 cm in length and 0.30 MPa in pressure	Solid target, 500 μg/cm^2 in thickness	Gas target, 3.0 cm in length and 0.25 MPa in pressure
Beam (μA)	2.5	2.5	2.5
Beam duration (h)	73	99	24 (three energies)
Accelerator	PKU 4.5-MV Van de Graaff accelerator		CIAE HI-13 tandem accelerator

angular differential cross sections were taken from Refs. [16] and [17], respectively.

Since it was difficult to obtain monoenergetic neutrons in the 7–13 MeV region, the subtraction of the interference from the low-energy neutrons, which was one of the most important reasons for the large deviations among existing experiments in the 7–13 MeV region, was required. In the present paper, because the cross sections of the ^{238}U(n,f) reaction induced by low-energy neutrons are apparently lower than those induced by the main neutrons, the uncertainty caused by the correction of the interference from the low-energy neutrons is restricted. After subtracting the interference from the low-energy neutrons, the average fluence of the main neutrons through the ^{238}U sample can be determined. With the corresponding D$(d,n)^3$He or ^{9}Be$(\alpha,n_0)^{12}$C angular differential cross sections, the ratio G [18] of the main neutron average fluence through the ^{238}U sample over that through the ^{56,54}Fe samples is calculated. It should be pointed out that the interference from the low-energy neutrons to the measured α events emitted from the ^{56,54}Fe$(n,\alpha)^{53,51}$Cr reactions can be ignored for two reasons. First, the energies of the α particles induced by low-energy neutrons are lower than the measurement threshold (as shown in Fig. 5). Second, the α particles induced by low-energy neutrons are scarce since the corresponding cross sections are small.

A twin gridded ionization chamber was used as the charged particle detector [19]. The separations of the cathode grid and the grid anode were 61 and 15 mm, respectively. The distance from the anode to the fission cathode (or to the shielding electrode) was 9 mm. The working gas was Xe +5% H_2 mixtures and the pressures were 0.052 MPa at 5.5 MeV, 0.072 MPa at 7.7 MeV, and 0.095 MPa at 8.5–10.5 MeV, separately. The cathode of the chamber contained a sample changer with five sample positions and back-to-back samples can be mounted at each of them. At four sample positions, back-to-back ^{56}Fe samples, ^{54}Fe samples, Ta backings, and compound α sources were mounted, individually. The samples can be replaced through rotating a knob below the chamber without opening it [19]. The details of the highly enriched (99.9%) ^{56}Fe and ^{54}Fe foil samples were presented in Ref. [1]. The radii of the ^{56}Fe and ^{54}Fe foil samples ranged from 21.5 to 23.0 mm and the corresponding thickness ranged from 0.54 to 0.58 mg/cm^2. The thickness of the Ta backing was 0.1 mm.

The data acquisition system was similar to that presented in Ref. [10]. The coincident anode-cathode signal pulses were recorded by the two waveform digitizers (Signatec PDA14, 100 MHz in sampling rate) for the forward and the backward directions, respectively. After correcting the baseline of the recorded signal pulses and then smoothing the signal pulses, the amplitudes of both the cathode and anode signals of the corresponding event were decided. The amplitudes of the fission signals were recorded by the desktop digitizer (CAEN DT5730B, 500 MHz in sampling rate).

At each energy point, five runs of measurements were performed. First, the experimental setup was calibrated using the compound α sources, the result of which is shown in Fig. 3. Second and third, the ^{56}Fe and ^{54}Fe samples were measured (foreground), separately. Fourth, the Ta backings were measured (background). Finally, the experimental setup was calibrated again to check its stability. The beam durations are shown in Table I, the total of which is ∼196 h.

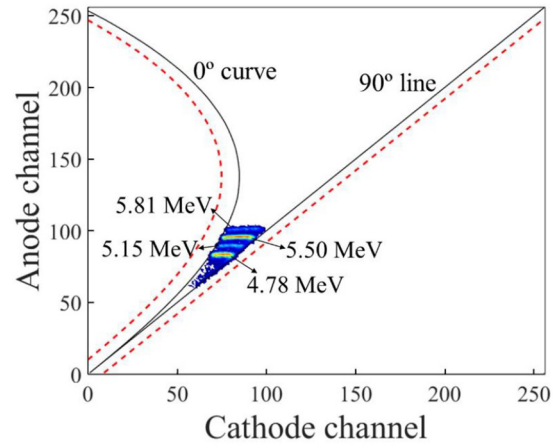

FIG. 3. The measured cathode-anode two-dimensional spectrum of the compound α source in the forward direction.

III. DATA PROCESSING AND THE RESULTS

The calibration using the compound α sources not only can decide the energy for each anode channel but also can decide the effective area of the α events. As an example shown in Fig. 3, the energy of each anode channel can be decided by the four α energy groups, and the effective area of the α events is located between the two dashed curves shown in Fig. 3. Considering that the energy resolution is smaller in the measurement with the neutron beam on, the effective area is larger than the region between the 0° curve and the 90° line.

The net α events are obtained using the foreground deducting the background, and the ratio of the fission count in the measurement of the foreground over that in the measurement of the background is used as the normalization factor of the neutron fluence. As an example, Fig. 4 presents the cathode-anode two-dimensional spectrum after the background

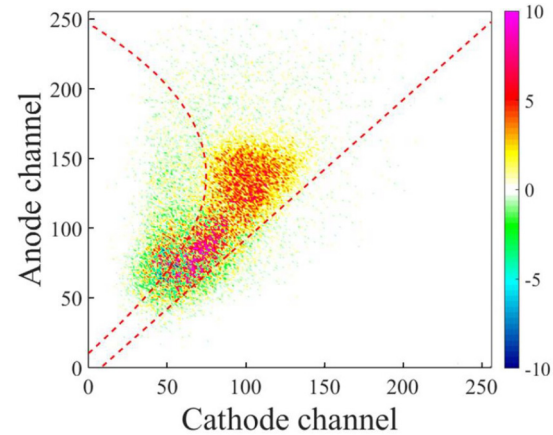

FIG. 4. The cathode-anode two-dimensional spectrum after the background deduction in the forward direction for the measurement of the ^{54}Fe$(n,\alpha)^{51}$Cr reaction at $E_n = 8.5$ MeV.

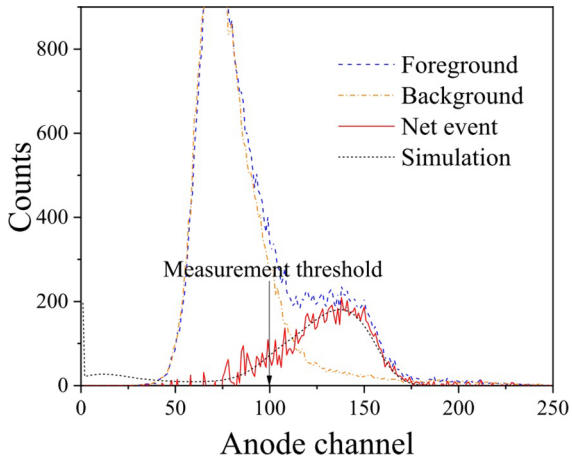

FIG. 5. The measured anode spectra of the ^{54}Fe$(n,\alpha)^{51}$Cr reaction at $E_n = 8.5$ MeV in the forward direction compared with the simulated one.

deduction in the measurement of the ^{54}Fe$(n,\alpha)^{51}$Cr reaction at $E_n = 8.5$ MeV. In the effective area between the two dashed curves in Fig. 4, the events are projected to the anode channel and counted as shown in Fig. 5. Since the residual nuclei are often in the excited states, the effective Q value is negative in most cases. So the interference from the background is still significant even if the working gas is Xe + 5% H_2 mixtures as shown in Fig. 5.

The detection efficiency of the α events is determined using Monte Carlo simulation. In the simulation, the corresponding double differential cross sections calculated utilizing TALYS-1.8 code [20] and the stopping powers calculated by SRIM-2013 code [21] are used and the result is shown in Fig. 5 as "Simulation". It should be pointed out that the counts of the simulated anode spectra may be higher or lower than the measured ones because the calculated cross sections may be inaccurate, so each of the simulated anode spectra is multiplied by a factor to fit the measurements.

The measured (n,α) cross section σ can be determined by

$$\sigma = \frac{N_{\rm U} N_{{\rm d}\alpha} \varepsilon_f G}{N_{\rm Fe} N_{{\rm d}f} (1-\rho_L) \varepsilon_\alpha} \sigma_f, \quad (1)$$

where $N_{\rm U}$ and $N_{\rm Fe}$ are the nucleus numbers of the ^{238}U and the ^{56,54}Fe samples, separately; $N_{{\rm d}f}$ and $N_{{\rm d}\alpha}$ are the detected (n,f) and (n,α) events, individually; ρ_L is the proportion of the (n,f) events induced by low-energy neutrons; ε_f and ε_α are the detection efficiencies of the (n,f) and (n,α) events, respectively; G is the ratio of the average fluence of the main neutrons through the ^{238}U sample over that through the ^{56,54}Fe samples [18]; and σ_f is the ^{238}U(n,f) cross section taken from Ref. [14]. Each of these quantities will induce more or less uncertainty to the measured cross sections as listed in Table II. The measured ^{56,54}Fe$(n,\alpha)^{53,51}$Cr cross sections are illustrated in Table III and Figs. 6 and 7. Among the existing measurements, Wang *et al.* [1] is our previous measurement, which agrees well with the present results and thus verifies the reliability of our measurements.

TABLE II. Sources of the uncertainty and their magnitudes.

Source	Magnitude (%)	Source	Magnitude (%)
$N_{\rm U}$	0.5	ε_α	0.4–2.5
$N_{\rm Fe}$	1.0	G	3.3–4.3
$N_{{\rm d}\alpha}$	2.1–11.4	ρ_L	0.2–3.6
$N_{{\rm d}f}$	0.1–0.4	σ_f	0.8–1.0
ε_f	1.0–1.2	Total	4.6–12.4

For the ^{56}Fe$(n,\alpha)^{53}$Cr reaction, apart from our present and previous (Wang *et al.* [1]) results, only one measured point at 8.0 MeV (Saraf *et al.*) is included in the EXFOR library [5], which is apparently lower than ours. To help constrain the excitation function more accurately, the ^{56}Fe$(n,x\alpha)$ cross sections (Grimes *et al.* [22], Fischer *et al.* [23], and Sterbenz *et al.* [24]) are used. According to the ratio of the ^{56}Fe$(n,\alpha)^{53}$Cr cross section over the ^{56}Fe$(n,x\alpha)$ cross section taken from the JENDL-4.0 library [6], the ^{56}Fe$(n,\alpha)^{53}$Cr cross sections are calculated from the ^{56}Fe$(n,x\alpha)$ cross sections (shown in Fig. 6 as "Calculated"). Since the abundance of ^{56}Fe in natural iron is as high as 91.754% and the differences among the cross sections of different isotopes of iron are not extremely significant, the cross sections of the natural iron are close to those of ^{56}Fe. Thus, the (n,α) cross sections of the natural iron measured by Paulse *et al.* [5] and Wattecamos *et al.* [5] and the $(n,x\alpha)$ cross sections of natural iron measured by Baba *et al.* [25] and Kunieda *et al.* [26] (shown in Fig. 6 as "Nat") are also presented and compared with the presented results. The present ^{56}Fe$(n,\alpha)^{53}$Cr cross sections agree well with the calculated results of Sterbenz *et al.* [24]. Also, the results of Paulse *et al.* [5] agree with the present results except for the two energy points above 9 MeV, and the results of Baba *et al.* [25] agree with the present results except for the measured point at 7.9 MeV. As illustrated in Fig. 6, the present ^{56}Fe$(n,\alpha)^{53}$Cr cross sections show a shoulder structure in the 8–11 MeV region, but most evaluations do not show this shoulder structure. In addition to the present measurements, the results of Sterbenz *et al.* [24] and Baba *et al.* [25] also show the shoulder structure although the shoulder in Sterbenz *et al.* [24] is not very clear. In addition, the evaluation of CENDL-3.1 also supports this shoulder structure although the shoulder is not apparent.

TABLE III. Measured ^{56,54}Fe$(n,\alpha)^{53,51}$Cr cross sections compared with those calculated using TALYS-1.8 code with adjusted input parameters.

E_n(MeV)	^{56}Fe		^{54}Fe	
	$\sigma_{\rm exp}$(mb)	$\sigma_{\rm TALYS}$(mb)	$\sigma_{\rm exp}$(mb)	$\sigma_{\rm TALYS}$(mb)
5.5	1.02 ± 0.13	1.01	3.76 ± 0.24	4.52
7.7	9.26 ± 1.07	10.93	28.69 ± 2.23	28.12
8.5	14.99 ± 0.83	15.00	35.66 ± 1.62	35.31
9.5	21.77 ± 1.70	20.64	41.31 ± 2.05	41.01
10.5	23.46 ± 2.92	24.06	43.77 ± 3.52	46.07

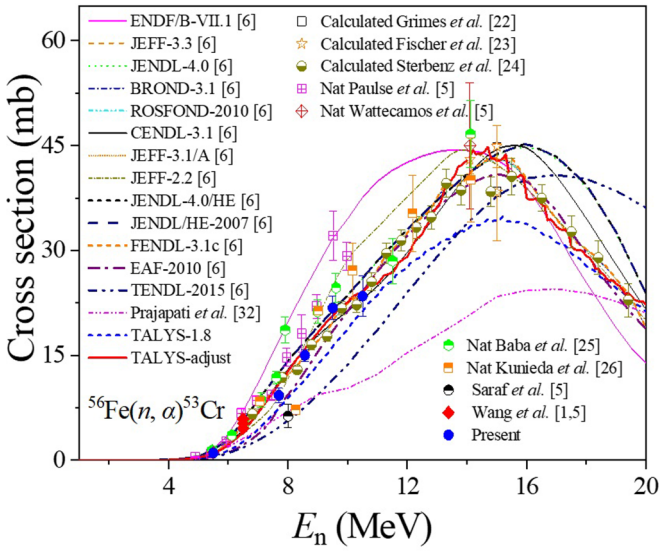

FIG. 6. The present ^{56}Fe$(n,\alpha)^{53}$Cr cross sections compared with the existing measurements and evaluations. Among the measured cross sections, only Saraf *et al.* and Wang *et al.* are included in the EXFOR library [5], and the others are the calculated results based on the measured ^{56}Fe$(n,x\alpha)$ cross sections. In addition, the (n,α) cross sections of natural iron measured by Paulse *et al.* [5] and Wattecamos *et al.* [5], and the $(n,x\alpha)$ cross sections of natural iron measured by Baba *et al.* [25] and Kunieda *et al.* [26] are also presented.

Because there is no newly opened reaction channel [such as $(n,2n)$ and (n,np)] with a large cross section in this neutron energy region, the measured shoulder structure may be caused by the level structure of the residual ^{53}Cr. Since both the neutron number 29 and proton number 24 in ^{53}Cr are close to the magic number 28, the level structure is in "concave"

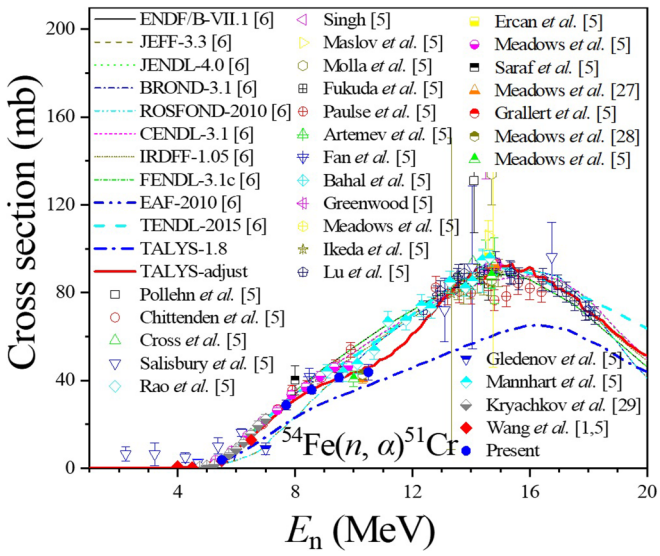

FIG. 7. The present ^{54}Fe$(n,\alpha)^{51}$Cr cross sections compared with the existing measurements and evaluations. All the measurements are included in the EXFOR library [5] except for Meadows *et al.* [27,28] and Khryachkov *et al.* [29].

TABLE IV. Adjusted input parameters of TALYS-1.8.

^{56}Fe		^{54}Fe	
Keyword	Parameter	Keyword	Parameter
preeqmode	4	preeqmode	4
aadjust	26 57 1.28	maxlevelsbin	a 15
maxlevelsbin	a 22	pair	24 51 1 .90
pair	24 53 2.70	gammald	24 51 0.55
gammald	24 53 0.80	Tadjust	24 51 0.72
Tadjust	24 53 0.58	E0adjust	24 51 0.44
E0adjust	24 53 0.46	avadjust	a 1.02
avadjust	a 1.18	cstrip	a 1.15
cstrip	a 1.50	pair	25 54 0.55
Tadjust	25 56 0.58	E0adjust	25 54 0.90
avadjust	p 0.85	avadjust	p 1.12
		Tadjust	26 53 1.10

shape in the MeV region according to Ref. [30]. Larson and Dickens [31] also declared that the level structure of ^{53}Cr is not as well understood as expected. In addition, Prajapati *et al.*'s calculation [32] also supports that the level structure may induce this shoulder structure in the 8–11 MeV region, because their calculation using the microscopic level densities from Hilaire's table presents a shoulder structure although the cross section is about a factor of 0.5 smaller (shown in Fig. 6 as "Prajapati *et al.* [32]"). Through adjusting several input parameters, most of which are related with the level density as listed in Table IV, the calculated ^{56}Fe$(n,\alpha)^{53}$Cr excitation function using TALYS-1.8 code [20] agrees with the measurements as shown in Fig. 6. It should be mentioned that the shoulder structure of the ^{56}Fe$(n,\alpha)^{53}$Cr reaction is not conclusively decided due to the experimental uncertainty and the lack of measurements. To validate the shoulder structure of this reaction, more measurements are required.

The present ^{54}Fe$(n,\alpha)^{51}$Cr cross sections agree with most existing measurements, and the results indicate that there may be some deviations among the measurements of Salisbury *et al.* [5], Paulsen *et al.* at 9.9 MeV [5], and Gledenov *et al.* [5]. The present results validate the shoulder structure in the 8–11 MeV region, which is absent in most evaluations. Being the same as the ^{56}Fe$(n,\alpha)^{53}$Cr reaction, the measured shoulder structure may be caused by the level structure of the residual ^{51}Cr because the level structure of ^{51}Cr is also in concave shape in the MeV region [30]. Through adjusting several input parameters as listed in Table IV, the ^{54}Fe$(n,\alpha)^{51}$Cr excitation function calculated using TALYS-1.8 code [20] also agrees with the measurements as presented in Fig. 7.

According to Schulc *et al.*'s [7] method utilized to validate the evaluated ^{54}Fe$(n,\alpha)^{51}$Cr excitation function using the integral reaction rates in the 0.8–20 MeV region induced by a ^{252}Cf neutron source, the evaluations of ENDF/B-VII.1, JENDL-4, and CENDL-3.1 libraries are higher than Schulc *et al.*'s measurement by 12.7–17.6%, while the result of the present calculation agrees with Schulc *et al.*'s measurement within the uncertainty. The main differences between the present calculation and those evaluations are located in the 8–14 MeV region, which means that the present measurements

and calculations in this region are reliable, i.e., the shoulder structure should exist.

It is interesting to notice that the shoulder structure is also observed in the measured (n, α) cross sections of several other nuclei near ^{56,54}Fe, such as ^{58}Ni [26,33], ^{59}Co [5], and ^{53,50}Cr [29]. This indicates that the level structure of the nuclei around ^{56,54}Fe may be significantly affected by the shell effect.

Other major reaction channels for neutron induced ^{56}Fe and ^{54}Fe reactions are also checked. The differences between the results of the calculations of the (n, tot) and (n, el) reactions with and without adjusting the input parameters can be ignored and the results agree with the measurements well. The calculated (n, n'), (n, p), and $(n, 2n)$ excitation functions with adjusting the input parameters agree much better with the measurements and evaluations than those without adjusting the input parameters. This verifies the adjustment of the input parameters.

IV. CONCLUSIONS

The cross sections of the ^{56,54}Fe$(n, \alpha)^{53,51}$Cr reactions were measured in the 5–11 MeV region at five neutron energy points, and the present results illustrate a shoulder structure for both reactions. Through adjusting several input parameters, mostly related with the level density, the excitation functions of these two reactions calculated using TALYS-1.8 code agree well with the measurements. The present results are helpful to constrain the ^{56,54}Fe$(n, \alpha)^{53,51}$Cr excitation functions, and they are useful to clarify the deviations among the existing measurements and evaluations. Especially in the neutron energy region of 8–11 MeV, the meaning of the present results is significant because the existing measurements are nonexistent or scarce and the deviations among existing measurements and evaluations are very large. The present results indicate that the related measurements are still required to constrain the excitation functions, especially in the 10–14 MeV region. Furthermore, the measurements for the isotopes of Fe and of the elements near Fe (e.g., Cr, Mn, Co, and Ni) are also very meaningful to study the shoulder structure because the shoulder structure is also observed in the (n, α) reactions of several isotopes of the elements near Fe.

ACKNOWLEDGMENTS

The authors are indebted to the operation crews of the 4.5-MV Van de Graaff accelerator of Peking University and of the Beijing HI-13 Tandem Accelerator of China Institute of Atomic Energy. Prof. Hanlin Lu and Prof. Zuying Zhou from CIAE, Prof. Naohiko Otsuka from IAEA, and Prof. Zhenpeng Chen from Tsinghua University are acknowledged for their helpful suggestions. The present work is financially supported by the National Natural Science Foundation of China (Grants No. 11475007 and No. 11775006), Science and Technology on Nuclear Data Laboratory, and China Nuclear Data Center.

[1] Z. Wang, X. Fan, L. Zhang, H. Bai, J. Chen, G. Zhang, Yu. M. Gledenov, M. V. Sedusheva, L. Krupa, and G. Khuukhenkhuu, Phys. Rev. C **92**, 044601 (2015).
[2] Z. Chen, X. Zhang, Y. Chen, G. Tang, G. Zhang, Yu. M. Gledenov, G. Khuukhenkhuu, and M. V. Sedusheva, Nucl. Phys. Rev. **16**, 31 (1999) (in Chinese).
[3] P. V. Rao and R. W. Fink, Phys. Rev. **154**, 1023 (1967).
[4] N. Fotiades, R. O. Nelson, and M. Devlin, Phys. Rev. C **81**, 037304 (2010).
[5] EXFOR: Experimental Nuclear Reaction Data, https://www-nds.iaea.org/exfor/exfor.htm.
[6] ENDF: Evaluated Nuclear Data File, https://www-nds.iaea.org/exfor/endf.htm.
[7] M. Schulc, M. Košťál, S. Simakov, V. Rypar, D. Harutyunyan, J. Šimon, N. Burianová, E. Novák, B. Jánský, M. Mareček, and J. Uhlíř, Appl. Radiat. Isot. **132**, 29 (2018).
[8] J. W. Meadows, D. L. Smith, L. R. Greenwood, L. P. Geraldo, W. Mannhart, and G. Börker, *Nuclear Data for Science and Technology*, edited by S. M. Qaim (Springer, Berlin, 1992), p. 288.
[9] H. Bai, Z. Wang, L. Zhang, H. Jiang, Y. Lu, J. Chen, and G. Zhang, Nucl. Instrum. Methods Phys. Res. A **886**, 109 (2018).
[10] H. Bai, H. Jiang, Y. Lu, Z. Cui, J. Chen, and G. Zhang, Determination of the amount of ^{238}U target nuclei and simulation of the neutron induced fission fragment energy spectrum (unpublished).
[11] C. Ji, D. Huang, T. Wang, and Q. Zhang, J. Isotopes **28**, 93 (2015) (in Chinese).
[12] Z. Wang, H. Bai, L. Zhang, H. Jiang, Y. Lu, J. Chen, G. Zhang, Yu. M. Gledenov, M. V. Sedysheva, and G. Khuukhenkhuu, Phys. Rev. C **96**, 044621 (2017).
[13] G. Zhang, H. Wu, J. Zhang, J. Liu, J. Chen, Yu. M. Gledenov, M. V. Sedysheva, G. Khuukhenkhuu, and P. J. Szalanski, Eur. Phys. J. A **43**, 1 (2010).
[14] Neutron Cross-Section Standards, 2006, https://www-nds.iaea.org/standards/Data/standards-238U_xs-data.txt.
[15] S. Cabral, G. Börker, H. Klein, and W. Mannhart, Nucl. Sci. Eng. **106**, 308 (1990).
[16] J. R. Risser, J. E. Price, and C. M. Class, Phys. Rev. **105**, 1288 (1957).
[17] V. G. Kiptily, A. V. Matyukov, A. S. Mishin, V. O. Naidenov, I. A. Polunovsky, L. A. Rassadin, and I. N. Chugunov, Bull. Russ. Acad. Sci.: Phys. **56**, 738 (1992).
[18] G. Zhang, Yu. M. Gledenov, G. Khuukhenkhuu, M. V. Sedysheva, P. J. Szalanski, P. E. Koehler, Yu. N. Voronov, J. Liu, X. Liu, J. Han, and J. Chen, Phys. Rev. Lett. **107**, 252502 (2011).
[19] X. Zhang, Z. Chen, Y. Tang, J. Yuan, G. Tang, G. Zhang, J. Chen, Yu. M. Gledenov, G. Khuukhenkhuu, and M. Sedysheva, Phys. Rev. C **61**, 054607 (2000).
[20] A. Koning, S. Hilaire, and S. Goriely, *User Manual of TALYS-1.8* (Nuclear Research and Consultancy Group, Petten, 2015).
[21] J. F. Ziegler, SRIM-2013, http://www.srim.org/#SRIM.
[22] S. M. Grimes, R. C. Haight, K. R. Alvar, H. H. Barschall, and R. R. Borchers, Phys. Rev. C **19**, 2127 (1979).
[23] R. Fischer, G. Traxler, M. Uhl, and H. Vonach, Phys. Rev. C **30**, 72 (1984).

[24] S. M. Sterbenz, F. B. Bateman, T. M. Lee, R. C. Haight, P. G. Young, M. B. Chadwick, F. C. Goeckner, C. E. Brient, S. M. Grimes, P. Maier-Komor, and H. Vonach, *Proceedings of the International Conference Nuclear Data for Science and Technology, Gatlingurg, Tennessee, May 9-13, 1994*, edited by J. K. Dickens (American Nuclear Society, Inc., La Grange Park, Illinois, 1994), Vol. 1, pp. 314–317.

[25] M. Baba, N. Ito, I. Matsuyama, S. Matsuyama, N. Hirakawa, S. Chiba, T. Fukahori, M. Mizumoto, K. Hasegawa, and S. Meigo, J. Nucl. Sci. Technol. **31**, 745 (1994).

[26] S. Kunieda, R. C. Haight, T. Kawano, M. B. Chadwick, S. M. Sterbenz, F. B. Bateman, O. A. Wasson, S. M. Grimes, P. Maier-Komor, H. Vonach, T. Fukahori, and Y. Watanabe, Phys. Rev. C **85**, 054602 (2012).

[27] J. Meadows, D. Smith, L. Greenwood, R. C. Haight, Y. Ikeda, and C. Konno, Measured fast-neutron activation cross sections of Ag, Cu, Eu, Fe, Hf, Ni, Tb and Ti at 10.3 and 14.8 MeV and for the continuum neutron spectrum produced by 7-MeV deuterons on a thick Be-metal target, Technical Report, 1991, https://digital.library.unt.edu/ark:/67531/metadc1103824/.

[28] J. Meadows, D. Smith, L. Greenwood, R. C. Haight, Y. Ikeda, and C. Konno, International Nuclear Data Committee, INDC(NDS)-286 (1993), p. 13.

[29] V. Khryachkov, A. Gurbich, T. Khromyleva, I. Bondarenko, V. Ketlerov, and P. Prusachenko, EPJ Web Conf. **146**, 11017 (2017).

[30] M. Maruyama, Nucl. Phys. A **131**, 145 (1969).

[31] D. C. Larson and J. K. Dickens, Phys. Rev. C **39**, 1736 (1989).

[32] P. M. Prajapati, Bhawna Pandey, C. V. S. Rao, S. Jakhar, T. K. Basu, B. K. Nayak, S. V. Suryanarayana, and A. Saxena, Fusion Sci. Technol. **66**, 426 (2014).

[33] V. V. Ketlerov, A. A. Goverdovskiy, V. F. Mitrofanov, Y. B. Ostapenko, and V. Y. Khryachkov, Vop. At. Nauki Tekhn. Ser. Yadernye Konstanty **1**, 121 (1996) (in Russian).